Developmental Cell *10*, 563–573, May, 2006 ©2006 Elsevier Inc. DOI 10.1016/j.devcel.2006.03.004

Combined Loss of Cdk2 and Cdk4 Results in Embryonic Lethality and Rb Hypophosphorylation

Cyril Berthet,[1] Kimberly D. Klarmann,[2] Mary Beth Hilton,[1] Hyung Chan Suh,[2] Jonathan R. Keller,[2] Hiroaki Kiyokawa,[3] and Philipp Kaldis[1,*]

[1] National Cancer Institute
Mouse Cancer Genetics Program
NCI-Frederick
Building 560/22-56
[2] Basic Research Program
Science Applications International Corporation
NCI-Frederick
Building 560
1050 Boyles Street
Frederick, Maryland 21702
[3] Northwestern University
Feinberg School of Medicine
Department of Molecular Pharmacology and Biological Chemistry
303 East Chicago Avenue
Chicago, Illinois 60611

Summary

Mouse knockouts of Cdk2 and Cdk4 have demonstrated that, individually, these genes are not essential for viability. To investigate whether there is functional redundancy, we have generated double knockout (DKO) mice. *Cdk2*$^{-/-}$ *Cdk4*$^{-/-}$ DKOs die during embryogenesis around E15 as a result of heart defects. We observed a gradual decrease of Retinoblastoma protein (Rb) phosphorylation and reduced expression of E2F-target genes, like Cdc2 and cyclin A2, during embryogenesis and in embryonic fibroblasts (MEFs). DKO MEFs are characterized by a decreased proliferation rate, impaired S phase entry, and premature senescence. HPV-E7-mediated inactivation of Rb restored normal expression of E2F-inducible genes, senescence, and proliferation in DKO MEFs. In contrast, loss of *p27* did not rescue *Cdk2*$^{-/-}$ *Cdk4*$^{-/-}$ phenotypes. Our results demonstrate that Cdk2 and Cdk4 cooperate to phosphorylate Rb in vivo and to couple the G1/S phase transition to mitosis via E2F-dependent regulation of gene expression.

Introduction

Cell proliferation is controlled by cyclin-dependent kinases (Cdks) (for review, see Malumbres and Barbacid, 2005; Morgan, 1997). The sequential phosphorylation of the retinoblastoma protein (Rb) plays a pivotal role in the G1/S phase transition (Bartek et al., 1996; Mittnacht, 1998; Weinberg, 1995; Zarkowska et al., 1997). In its hypophosphorylated state, Rb sequesters and represses the E2F family of transcription factors (Weinberg, 1995). Mitogenic growth factors induce phosphorylation of Rb by activation of cyclin D-Cdk4/6 and cyclin E/Cdk2 complexes. This results in release of E2F proteins from Rb and promotes transcriptional activation of genes required for S phase and DNA replication (Ezhevsky et al., 2001; Harbour and Dean, 2000; Harbour et al., 1999; Lundberg and Weinberg, 1998). Conversely, growth-inhibitory signals reduce cyclin levels or induce Cdk inhibitors (CKIs), resulting in decreased cyclin/Cdk activity, hypophosphorylation of Rb, and, subsequently, in repression of E2F-target genes (for review, see Ruas and Peters, 1998; Sherr, 2001; Sherr and Roberts, 1999).

Mouse models have been developed in order to better understand the G1/S transition of the cell cycle and the interplay of the cyclin/Cdk complexes. Inactivation of individual genes encoding members of these complexes (cyclins D1, D2, D3, E1, and E2 and Cdk2, Cdk4, and Cdk6) has revealed that none of these proteins considered to be important for the control of the G1/S transition are essential for viability per se and that their loss causes few cell cycle defects (Berthet et al., 2003; Fantl et al., 1995; Geng et al., 2003; Malumbres et al., 2004; Ortega et al., 2003; Parisi et al., 2003; Rane et al., 1999; Sicinski et al., 1995, 1996; Tsutsui et al., 1999). For example, male and female *Cdk2*$^{-/-}$ mice are sterile but otherwise comparable to wild-type mice. Mouse embryonic fibroblasts (MEFs) derived from *Cdk2*$^{-/-}$ embryos display a delayed entry into S phase and are not efficiently immortalized (Berthet et al., 2003; Ortega et al., 2003). *Cdk4*$^{-/-}$ mice are substantially smaller compared to wild-type mice, develop diabetes spontaneously, and are sterile (Rane et al., 1999; Tsutsui et al., 1999). *Cdk4*$^{-/-}$ MEFs display a delayed entry into S phase concomitant with low Cdk2 activity due to increased p27 binding. This defect is partially rescued by the loss of *p27* (Tsutsui et al., 1999).

Further studies used double (DKO) or triple knockout (TKO) mice to characterize in vivo functions of each subfamily (D-type cyclins, E-type cyclins, Cdk4/Cdk6) and potential compensatory mechanism. Indeed, ablation of the three D-type cyclins leads to embryonic lethality around E15.5, which is associated with a cardiac output failure and severe anemia (Kozar et al., 2004). Similarly, inactivation of *Cdk4* and *Cdk6*, partners of D-type cyclins, results in a late embryonic lethality with severe anemia (Malumbres et al., 2004). Both models indicate that D-type cyclin/Cdk4 and cyclin/Cdk6 complexes are involved in development of the hematopoietic lineage, but that, overall, they have little effect on cell proliferation and organogenesis. Analysis of MEFs confirmed that inactivation of Cdk4 and Cdk6 or D-type cyclins delays S phase entry (or reentry after serum starvation) but does not prevent proliferation (Kozar et al., 2004; Malumbres et al., 2004). In contrast, *cyclin E1*$^{-/-}$*E2*$^{-/-}$ DKO MEFs proliferate, but they fail to exit quiescence owing to a defect in loading of MCM proteins onto DNA prereplication complexes (Geng et al., 2003). In vivo, DKOs of cyclins E1 and E2 result in embryonic lethality due to defective trophoblast endoreplication (Geng et al., 2003; Parisi et al., 2003). All of these findings suggest that D-type or E-type cyclin complexes are not essential for proliferation in vivo and in vitro (with the exception of exit from quiescence for E-type cyclins), and that these complexes

*Correspondence: kaldis@ncifcrf.gov

might need to be inactivated simultaneously to affect cell cycle progression. As a first approach, Malumbres et al. (2004) have generated *Cdk2*$^{-/-}$*Cdk6*$^{-/-}$ mice, which are viable and do not exhibit cell cycle defects. However, silencing of Cdk2 in *Cdk4*$^{-/-}$*Cdk6*$^{-/-}$ MEFs significantly affected the proliferation rate, indicating that at least one of these Cdks is required for the G1/S transition.

Cdk2 and *Cdk4* are located on the same chromosome, which renders the generation of DKOs difficult. We were able to generate *Cdk2*$^{-/-}$*Cdk4*$^{-/-}$ mice, and, interestingly, they exhibit embryonic lethality and cell cycle defects, unlike *Cdk2*$^{-/-}$*Cdk6*$^{-/-}$ mutants, which emphasize overlapping functions shared by Cdk2 and Cdk4.

Results

Generation of *Cdk2* and *Cdk4* DKO Mice

Cdk2 and *Cdk4* are located on chromosome 10D3 and are only 1.6 Mb apart (Figure 1A). We crossed *Cdk2*$^{+/-}$ with *Cdk4*$^{+/-}$ mice (Berthet et al., 2003; Tsutsui et al., 1999) to generate *Cdk2*$^{+/-}$*Cdk4*$^{+/-trans}$ mice and backcrossed those with C57BL/6 mice. Most of the resulting pups were heterozygous for *Cdk2* or *Cdk4*, except when a meiotic crossover occurred between the two gene loci. Meiotic crossovers occur at a frequency of 1% per 2 Mb distance in the mouse genome (Silver, 1995). In theory, 0.8% of animals generated from our backcrosses should be either wild-type or "*cis*" double heterozygous. We selected the latter animals, which carried both recombined loci in "*cis*" on chromosome 10 (Figure 1B). Out of 245 pups, we detected 3 double heterozygous and 3 wild-type mice; thus, we believe that a total of 2.4% recombination events occurred between these loci (Figure 1A). The chromosomal region 10D3 is close to the telomere, a region more susceptible to recombination, especially in males, which might explain the increased levels of recombination (Silver, 1995). We backcrossed *Cdk2*$^{+/-}$*Cdk4*$^{+/-cis}$ mice to confirm that both loci are linked and generated a colony for each founder. We then intercrossed *Cdk2*$^{+/-}$*Cdk4*$^{+/-cis}$ mice to generate *Cdk2*$^{-/-}$*Cdk4*$^{-/-}$ DKOs. Western blots from embryo extracts were performed and confirmed the absence of Cdk2 and Cdk4 proteins (Figure 1C).

In our crosses, we occasionally observed single heterozygosity for one gene associated with wild-type, or null locus for the other gene. These genotypes required a meiotic recombination to revert the link between *Cdk2* and *Cdk4* mutant loci. This reversion occurred at a frequency of 7%, suggesting, again, that this chromosomal region is highly susceptible to recombination. Among the offspring, we found some *Cdk2*$^{-/-}$*Cdk4*$^{+/-}$ or *Cdk2*$^{+/-}$*Cdk4*$^{-/-}$ mice, which were viable (data not shown).

Cdk2$^{-/-}$*Cdk4*$^{-/-}$ DKO Mice Are Embryonic Lethal

From the *Cdk2*$^{+/-}$*Cdk4*$^{+/-cis}$ intercrosses, no living *Cdk2*$^{-/-}$*Cdk4*$^{-/-}$ pups have been found; however, embryos lacking Cdk2 and Cdk4 were observed (Figure 1D). The embryonic lethality indicated that Cdk2 and Cdk4 have overlapping essential functions in vivo. Normal Mendelian ratios persisted until E13.5, but, at later stages, a significant percentage of *Cdk2*$^{-/-}$*Cdk4*$^{-/-}$ (DKO) embryos were found dead. Most, but not all, of the embryos died between E14.5 and E16.5

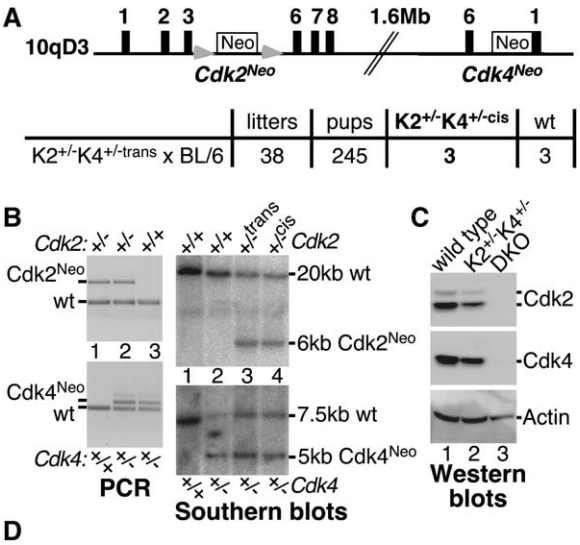

D

Embryonic stage	Observed ratio*	*Cdk2*$^{-/-}$*Cdk4*$^{-/-}$ alive embryos	*Cdk2*$^{-/-}$*Cdk4*$^{-/-}$ total embryos
E10.5-12.5	6 (1)/ 29	21%	24%
E13.5	30 (1)/ 105	29%	30%
E14.5	**19 (11)/ 154**	**12%**	**19%**
E15.5	**6 (12)/ 76**	**8%**	**24%**
E16.5	**6 (10)/78**	**8%**	**21%**
E17.5-18.5	2 (1)/ 51	4%	6%
Birth (P1)	0 (3)/ 72	0%	4%

Figure 1. Targeted Inactivation of *Cdk2* and *Cdk4* Genes

(A) Organization of the inactivated *Cdk2* and *Cdk4* loci after meiotic recombination and a table of the screening of *Cdk2*$^{+/-}$*Cdk4*$^{+/-trans}$ (K2$^{+/-}$K4$^{+/-}$) backcrossed to wild-type mice.

(B) Analysis of *Cdk2* and *Cdk4* loci. PCR analysis of genomic tail DNA from pups generated by backcrossing *Cdk2*$^{+/-}$*Cdk4*$^{+/-trans}$ mice. These pups were mostly single heterozygous for *Cdk2* (lane 1) or *Cdk4* (lane 3), and a few were double heterozygous *Cdk2*$^{+/-}$*Cdk4*$^{+/-cis}$ (lane 2). Southern blot analysis of tail genomic DNA from wild-type (lane 1), *Cdk4*$^{+/-}$ (lane 2), *Cdk2*$^{+/-}$*Cdk4*$^{+/-trans}$ (lane 3), and *Cdk2*$^{+/-}$*Cdk4*$^{+/-cis}$ (lane 4) mice. *Cdk2* 3′ probe and *Cdk4* 5′ probe were used as described in Experimental Procedures.

(C) Protein expression analysis by Western blots of Cdk2, Cdk4, and β-actin by using extracts of wild-type, *Cdk2*$^{+/-}$*Cdk4*$^{+/-}$ (K2$^{+/-}$K4$^{+/-}$), and DKO E13.5 embryos.

(D) Table for viability of *Cdk2*$^{-/-}$*Cdk4*$^{-/-}$ embryos at various stages of development. *Observed ratios correspond to the number of *Cdk2*$^{-/-}$*Cdk4*$^{-/-}$ embryos, alive (heart beating) and dead (in parentheses), compared to the total number of embryos harvested. *Cdk2* and *Cdk4* loci are linked; therefore, the expected percentage of *Cdk2*$^{-/-}$*Cdk4*$^{-/-}$ embryos is 25%. At E17.5 and later, most of the *Cdk2*$^{-/-}$*Cdk4*$^{-/-}$ embryos were dead and degraded, which precluded genotyping.

and displayed several gross phenotypes with incomplete penetrance: small size (80% for E14.5 and E15.5 embryos), pale color (26%), asymmetric ocular lesions (11%), and hemorrhagic edema (14%) (Figure 2A and Figure S1 in the Supplemental Data available with this article online). Histopathology analysis of serial sections revealed cardiovascular defects in all living E14.5–E16.5 embryos analyzed (Figure 2B, [c] and [d]), whereas no major abnormality was observed in other organs, including the placenta (data not shown). Cardiac morphogenesis appeared normal at E12.5 (data not shown), but

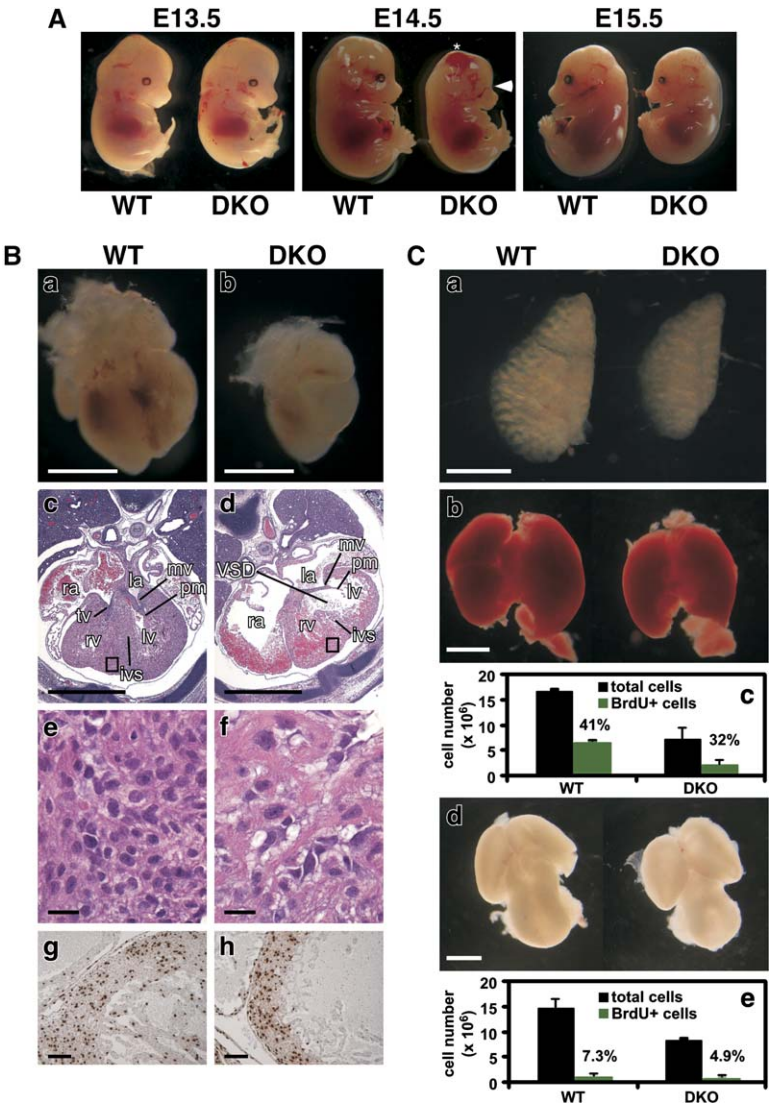

Figure 2. Phenotype of *Cdk2*$^{-/-}$*Cdk4*$^{-/-}$ Mice

(A) Appearance of wild-type and *Cdk2*$^{-/-}$ *Cdk4*$^{-/-}$ embryos at the indicated stages of development. Wild-type littermates are shown for comparison. Eye defects (arrow) and edemas (*) occur with partial penetrance.

(B) Cardiovascular abnormalities in *Cdk2*$^{-/-}$ *Cdk4*$^{-/-}$ embryos. Appearance of isolated heart from (a) wild-type and (b) *Cdk2*$^{-/-}$ *Cdk4*$^{-/-}$ embryos at E14.5 (the scale bar is 1 mm). Histological transversal sections through the (c) wild-type and (d) *Cdk2*$^{-/-}$ *Cdk4*$^{-/-}$ heart in the plane of mitral valve (mv) and papillary muscle (pm). *Cdk2*$^{-/-}$ *Cdk4*$^{-/-}$ hearts display atrium enlargement, reduced thickness of the ventricle walls (compact zone), and an interventricular septum (ivs) with a ventricular septal defect (VSD) (the scale bar is 1 mm). Compact zone of (e) wild-type and (f) *Cdk2*$^{-/-}$*Cdk4*$^{-/-}$ ventricle walls from the boxed area in (c) or (d). Cardiomyocytes appear disorganized and hypertrophic in *Cdk2*$^{-/-}$*Cdk4*$^{-/-}$ embryos (the scale bar is 20 μm). Immunodetection of BrdU on transversal sections through hearts ([g] and [h]; the scale bar is 100 μm). The right atrium (ra), the left atrium (la), the right ventricle (rv), the left ventricle (lv), and the triscuspid valve (tv) are indicated.

(C) Organ size and BrdU incorporation in vivo (S phase marker). Whole mounts of (a) lungs, (b) liver, and (d) brain from E14.5 embryos are shown (the scale bar is 1 mm). Analysis by flow cytometry of BrdU-positive cells in (c) liver and (e) brain are depicted. The bar graph represents the absolute cell number per total fetal liver/brain and total BrdU-positive cells (percentage of BrdU-positive cells × total cells per fetal liver) for three wild-type or *Cdk2*$^{-/-}$*Cdk4*$^{-/-}$ embryos at E14.5.

it was severely affected at E14.5 (Figure 2B). Abnormalities included reduced global size (Figure 2B, [a] and [b]), enlargement of atria, thin ventricular walls, and hypertrophy of the valves. At the microscopic level, cardiomyocytes seem to be differentiated, but hypertrophic and disorganized (Figure 2B, [e] and [f]). Proliferation in certain areas of the heart was decreased in DKOs compared to wild-type (Figure 2B, [g] and [h]). These defects were most likely the origin of a cardiac output failure, sometimes triggering hemorrhages and, for most but not all of the *Cdk2*$^{-/-}$*Cdk4*$^{-/-}$ embryos, lethality before E16.5.

Among other observations, the small size of the *Cdk2*$^{-/-}$*Cdk4*$^{-/-}$ mutants was the most prevalent. Specific tissues, like lung, liver, or brain, indicated a size reduction as well (Figure 2C, [a], [b], and [d]). In order to characterize this phenotype, embryos isolated at different stages of development were examined for bromodeoxyuridine (BrdU) incorporation as a measure for DNA replication/S phase. We first pulse-labeled E14.5 embryos with BrdU and then prepared a cell suspension from liver or brain. The relative ratio of BrdU-positive cells was determined by flow cytometry, and the total number of BrdU-positive cells was calculated. We observed a 3-fold decrease of total BrdU-positive cells in liver (Figure 2C, [c]) and a 2.6-fold decrease of total BrdU-positive cells in brain (Figure 2C, [e]). This could be one reason for the low cellularity in the liver or brain and, most likely, for the similar defects existing in other tissues, which could result in global size reduction observed at E14.5 or at later stages. We also performed TUNEL staining on sections of limbs or heart/lung and detected comparable levels of apoptosis (see Figure S2), suggesting that the small size of *Cdk2*$^{-/-}$ *Cdk4*$^{-/-}$ embryos is probably linked to lower cell proliferation rather than to apoptosis.

Hematopoiesis in *Cdk2*$^{-/-}$*Cdk4*$^{-/-}$ Embryos

Knockouts of G1 phase regulators, like *Cdk4*$^{-/-}$*Cdk6*$^{-/-}$ DKOs and *cyclin D1*$^{-/-}$*D2*$^{-/-}$*D3*$^{-/-}$ TKOs, display severe hematopoietic defects (Kozar et al., 2004; Malumbres et al., 2004). A common feature of *Cdk2*$^{-/-}$*Cdk4*$^{-/-}$ embryos was their pale appearance, suggesting the possibility of hematopoietic abnormalities. To investigate the hematopoietic development in *Cdk2*$^{-/-}$*Cdk4*$^{-/-}$ embryos, we first examined fetal livers from wild-type and DKO embryos at E14.5, since this is the major

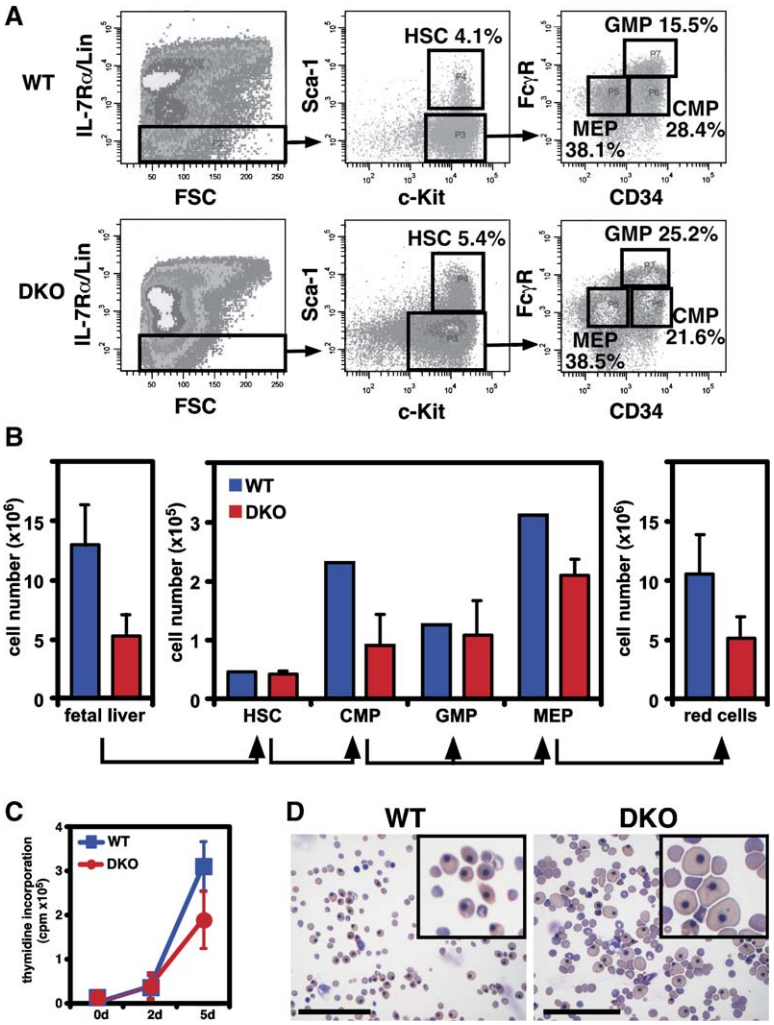

Figure 3. Hematopoietic Phenotype in *Cdk2*$^{-/-}$*Cdk4*$^{-/-}$ Embryos

(A) Flow cytometry analysis of hematopoietic stem cells (HSC), common myeloid progenitors (CMP), granulocyte-macrophage progenitors (GMP), and megakaryocyte-erythroid progenitors (MEP) isolated from E14.5 fetal livers. Relative percentages of selected populations are shown. FSC, forward scatter.

(B) Bar graphs represent absolute cell numbers per fetal liver or indicated subpopulations. Red cells were double positive for CD71 and TER119 staining. Error bars represent the standard deviation of 14 analyzed livers for the total cellularity and 3 different DKO data for the progenitors and red blood cells.

(C) ^{3}H-thymidine proliferation assay generated with cells isolated from total fetal liver and cultured in the presence of cytokines, enhancing multipotential progenitor growth. A total of 5×10^{3} cells were plated in triplicate in a 96-well plate and were pulsed with ^{3}H-thymidine after 2 and 5 days. Data are representative of three independent experiments analyzing seven fetal livers per genotype. Error bars represent the standard deviation of three different sets of data.

(D) Umbilical cord blood cells are shown. A total of 10^{5} cells were cytocentrifuged on slides and stained with Eosin/Azure A. The inset represents 2.3-fold magnification; the scale bar is 100 μm.

hematopoietic organ at this stage of development. We noticed that the cellularity was reduced 2.4-fold in DKOs compared to wild-type fetal livers (Figure 3B). To determine if low cellularity was associated with abnormal hematopoiesis, we used flow cytometry to distinguish various hematopoietic cell types, including erythroid cells, macrophages, granulocytes, and B cells (Figure 3B and data not shown). Similar percentages were observed for all of these mature hematopoietic cell types in wild-type and DKO fetal liver (data not shown). Thus, the reduction in liver cellularity reflects a loss in the total number of cells, which especially affects red blood cells (CD71+/TER119+) (Figure 3B), given that these cells represent 75% of the total cell population of fetal liver. This fact on its own likely accounts for the pale appearance of the DKO embryos. To investigate the reasons for the reduced number of *Cdk2*$^{-/-}$*Cdk4*$^{-/-}$ fetal liver cells, we analyzed cells in the following hematopoietic compartments: hematopoietic stem cells (HSC), which give rise to common myeloid progenitors (CMP) that, in turn, produce granulocyte-macrophage progenitors (GMP), and megakaryocyte-erythroid progenitors (MEP) (Akashi et al., 2000). We found that although the absolute number of hematopoietic progenitors was lower in DKO fetal livers, the relative percentages of all of these progenitors were not significantly different in DKOs compared to wild-type (Figures 3A and 3B). We next characterized the proliferation of the fetal liver cells by using a cytokine cocktail (mSCF, hFlt-3L, mIL-3, mIL-6) to enhance multipotential progenitor growth. A slight proliferation defect for DKO multipotential progenitors was detected by thymidine incorporation (Figure 3C). Nevertheless, the decreased growth rate did not affect the potential of progenitors to form colonies in soft agarose (WT, 16.2 ± 3; DKO, 14.8 ± 0.7; data not shown). We concluded that *Cdk2*$^{-/-}$*Cdk4*$^{-/-}$ hematopoietic cells are able to generate all progenitors and mature cells from HSC, but do so to a lesser extent than wild-type due to reduced proliferation of the multipotential progenitors, which, consequently, affects the amount of all other subpopulations.

To further characterize hematopoiesis in DKOs, we examined blood cells isolated from the umbilical cord of E14.5 embryos. As expected, fewer blood cells were harvested from the umbilical cord of *Cdk2*$^{-/-}$*Cdk4*$^{-/-}$ embryos (data not shown), although normal ratios of different subpopulations of blood cells were detected, in agreement with the flow cytometry analysis of fetal liver. We noticed that most nucleated erythroid cells from *Cdk2*$^{-/-}$*Cdk4*$^{-/-}$ mutants were larger than those isolated from wild-type (Figure 3D). These enlarged cells might represent primitive erythroblasts generated in

the yolk sack, which can persist until enough definitive erythroblasts have been generated (Kingsley et al., 2004).

Molecular Analysis of *Cdk2*$^{-/-}$*Cdk4*$^{-/-}$ Embryos

In order to investigate the basis of lethality in *Cdk2*$^{-/-}$*Cdk4*$^{-/-}$ embryos on a molecular level, we analyzed protein extracts from living (heart beating) embryos at E13.5, E14.5, or E16.5. We confirmed that Cdk2 and Cdk4 proteins are expressed during embryogenesis in wild-type embryos, but not in *Cdk2*$^{-/-}$*Cdk4*$^{-/-}$ embryos (Figure 4, first and second panels from top). The expression levels of p27 and Cdk6 were similar in wild-type and DKOs, with a slight decrease at E16.5 in DKOs (Figure 4, third and fourth panels from top). Cyclin D1 expression displayed the same pattern with a more pronounced decrease in DKOs at E16.5 (Figure 4, fifth panel from top). Interestingly, Cdc2 was expressed at a similar level at E13.5, but the expression of Cdc2 decreased progressively at E14.5 and E16.5 in *Cdk2*$^{-/-}$*Cdk4*$^{-/-}$ compared to wild-type embryos (Figure 4, sixth panel from top). The decreased Cdc2 expression is associated with a progressive reduction of Cdc2 activity (see Figure S3). We observed a similar expression pattern for cyclin A2 (Figure 4, sixth panel from bottom). Since Cdc2 and cyclin A2 are targets of E2F-mediated transcription, we next checked the status of Rb and E2F. Expression of E2F and Rb was comparable in all embryo extracts (Figure 4, fifth and third panels from bottom). In contrast, phosphorylation of Rb at serine 780, a Cdk4-specific site, was decreased at E14.5 and was undetectable at E16.5 in *Cdk2*$^{-/-}$*Cdk4*$^{-/-}$ compared to wild-type embryos (Figure 4, fourth panel from bottom). This result indicates that the phosphorylation of Rb requires Cdk2 or Cdk4; however, it also pointed out that, in early embryogenesis (before E14), other kinases can phosphorylate Rb (see Discussion). We immunoprecipitated cyclin D1 complexes from embryo extracts and observed more Cdk6 bound in DKOs compared to wild-type extracts at E13.5 and E14.5 (Figure 4, bottom panel). This result suggests that the absence of Cdk4 (and Cdk2) leaves cyclin D1 available for binding to Cdk6, which might compensate for, to a certain extent, the lack of Cdk4. At E16.5, this compensation was no longer observed due to the decreased expression of cyclin D1 (see fifth panel from top).

Proliferation of *Cdk2*$^{-/-}$*Cdk4*$^{-/-}$ Embryonic Fibroblasts

To evaluate the loss of Cdk2 and Cdk4 on a cellular level, we generated mouse embryonic fibroblasts (MEFs) to analyze cell proliferation and cell cycle regulation. At passage 2 (P2), *Cdk2*$^{-/-}$*Cdk4*$^{-/-}$ MEFs proliferated at a lower rate than did *Cdk2*$^{+/-}$*Cdk4*$^{+/-}$ (data not shown) or wild-type MEFs (Figure 5A, upper panel). At P4, proliferation of *Cdk2*$^{-/-}$*Cdk4*$^{-/-}$ MEFs was very low (Figure 5A, lower panel). To determine the percentage of cells in the different phases of the cell cycle, unsynchronized P2 MEFs were pulse labeled with BrdU and analyzed by flow cytometry. We found that 7% of the *Cdk2*$^{-/-}$*Cdk4*$^{-/-}$ cells were in S phase compared to 22% of the wild-type MEFs (see Figure S4), indicating a G1/S transition defect. To investigate the S phase entry defect further, MEFs were synchronized by contact inhibition/serum starvation, released into fresh medium,

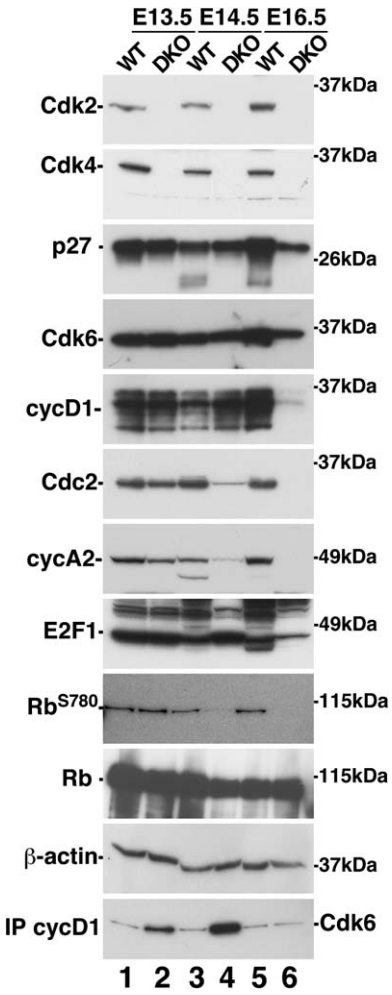

Figure 4. Molecular Analysis of *Cdk2*$^{-/-}$*Cdk4*$^{-/-}$ Embryos

Western blot analysis of extracts prepared from wild-type or living *Cdk2*$^{-/-}$*Cdk4*$^{-/-}$ embryos at E13.5, E14.5, and E16.5 with indicated antibodies. Immunoprecipitation of cyclin D1 followed by a Cdk6 Western blot is shown in the bottom panel.

labeled with BrdU, and analyzed by flow cytometry (Figure 5B). We found that wild-type cells began entering S phase at 15 hr after release (8.4% ± 0.3%) and reached a maximum after 24 hr (34.3% ± 2.3%). In contrast, only 2.7% ± 1.2% of the *Cdk2*$^{-/-}$*Cdk4*$^{-/-}$ MEFs were BrdU positive at 15 hr, and no more than 8.2% ± 1.1% positive cells were observed after 24 hr. This result indicates that the low proliferation rate of *Cdk2*$^{-/-}$*Cdk4*$^{-/-}$ MEFs, observed as early as P2, correlates with a reduced percentage of cells entering S phase. In parallel, we investigated whether DKO cells displayed senescent features (flat and enlarged morphology or senescent-associated [SA]-β-galactosidase staining; Dimri et al., 1995). A 2-fold increase of β-galactosidase-positive (blue) cells was observed in DKOs compared to wild-type MEFs at P2 and P4 (Figure 5C). Overall, these results suggest that loss of Cdk2 and Cdk4 affects cellular proliferation. Indeed, the lack of Cdk2 and Cdk4 influences S phase entry of MEFs at early passages and triggers premature senescence at late passages. Both defects result in a low proliferation rate, which decreases progressively with each passage in culture.

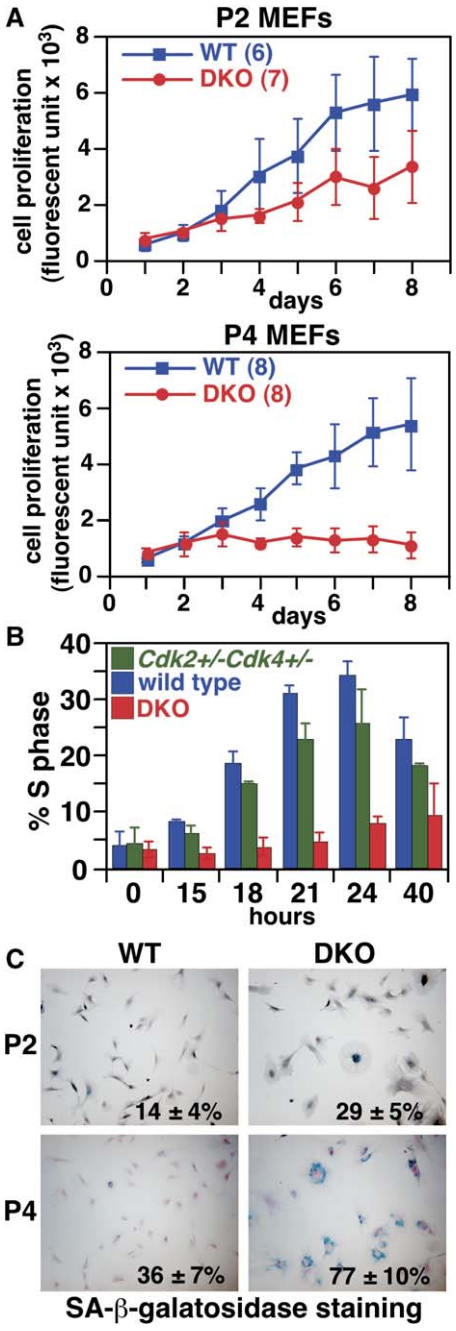

Figure 5. Cellular Proliferation in MEFs Lacking Cdk2 and Cdk4

(A) Proliferation of MEFs was analyzed for 8 days with AlamarBlue assays at passages 2 (upper panel) and 4 (lower panel). Error bars represent the standard deviation of the data from the clone number indicated in the figure: P2 WT (six clones), P2 DKO (seven clones), P4 WT (8 clones), P4 DKO (8 clones). Data represent the average of three clones (WT and $Cdk2^{+/-}Cdk4^{+/-}$) and six clones (DKO), respectively.

(B) S phase entry analysis of synchronized MEFs. After serum starvation, cells were released at time 0 hr and labeled with BrdU at the indicated time; the percentage of cells in S phase was determined by flow cytometry analysis.

(C) Senescent-associated (SA)-β-galactosidase staining of MEFs at passages 2 and 4. Cells were stained for SA-β-galactosidase after incubation for 24 hr. Data were the average compiled from three wild-type and five DKO clones; at least 200 cells were counted from each clone.

Rb/E2F Repression Contributes to Lack of Proliferation

Entry into S phase requires phosphorylation of Rb by cyclin/Cdk complexes whereupon phospho-Rb is released and E2F is activated (Trimarchi and Lees, 2002). Cdk2 and Cdk4 are among the kinases best characterized to phosphorylate Rb; however, recent in vivo studies have demonstrated the plasticity of Cdk redundancy, indicating that Cdc2 might compensate for Cdk2 (Aleem et al., 2005). In order to determine the molecular mechanism responsible for the $Cdk2^{-/-}Cdk4^{-/-}$ proliferation defects, we examined MEFs at P2 and P4 for the expression of Cdc2 complexes and E2F-target genes as we had done in embryo extracts (see Figure 4). We immunoprecipitated Cdc2 complexes and observed a decrease of Cdc2 protein expression level in DKO MEFs at P2; and this expression level was more pronounced at P4 (Figure 6A, top panel). Similarly, lower amounts of Cdc2 were detected in DKOs compared to wild-type MEFs after immunoprecipitation with Suc1, cyclin A2, or cyclin B1 antibodies (Figure 6A, second, third, and fourth panels from top). We also verified the expression levels of Rb, which was unchanged (Figure 6A, fourth panel from bottom), but phosphorylation of Rb at serine 780, serine 807/811, and threonine 821 was decreased in DKOs compared to wild-type MEFs (Figure 6A, bottom three panels). If E2Fs are not released from Rb, we should be able to observe inhibition of Cdc2 and expression of other E2F-target genes at the transcriptional level. Indeed, RT-PCR analysis indicated a decreased expression of *Cdc2*, *cyclin E2*, *cyclin A2*, *cyclin B1*, and *Cdc25A* mRNA in $Cdk2^{-/-}Cdk4^{-/-}$ MEFs compared to wild-type (Figure 6B, first, third, fourth, fifth, and sixth panels from top). This decrease was more accentuated at P4 than at P2. In contrast, *cyclin E1* expression was not affected (Figure 6B, second panel from top). Among the pocket proteins, *Rb* and *p130* were slightly downregulated, and *p107* expression was reduced in DKO MEFs (Figure 6B, seventh, eighth, and ninth panels from top). However, expression of Rb protein was comparable in wild-type and DKO MEFs, suggesting that molecular regulation of Rb is different than for other E2F-target genes. We have also examined the RNA expression of Cdk inhibitors and observed a similar increase of $p16^{INK4a}$ at P4 in wild-type and DKO MEFs, which probably reflects the senescence phenotype (Figure 6B, fifth panel from bottom). The levels of others Cdk inhibitors, $p19^{INK4d}$, $p21^{CIP1}$, and $p27^{KIP1}$, were decreased in DKOs compared to wild-type MEFs (Figure 6B, second, third, and fourth panels from bottom). A similar reduction of Cdk inhibitors has been observed in $Cdk4^{-/-}Cdk6^{-/-}$ MEFs (Malumbres et al., 2004), suggesting a feedback mechanism that reduces the overall levels of cell cycle inhibitors in the absence of normal levels of Cdks. Since E2F-target genes are responsible for entry into S phase and for cell cycle progression, the downregulation of *Cdc2* and other E2F-target genes in $Cdk2^{-/-}Cdk4^{-/-}$ MEFs likely accounts for the observed proliferation defects.

Rescue of Proliferation Defects in $Cdk2^{-/-}Cdk4^{-/-}$ MEFs

Our results so far indicate that there is a defect in the Rb/E2F pathway in DKO MEFs. To analyze this further, we wondered whether inactivation of Rb by expressing

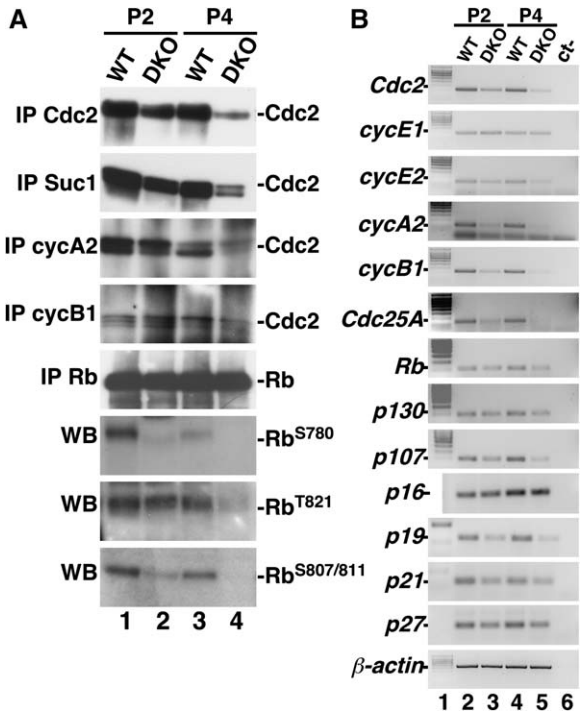

Figure 6. Expression of E2F-Target Genes in $Cdk2^{-/-}Cdk4^{-/-}$ MEFs

(A) Immunoprecipitations (IP) and Western blotting analysis of MEF extracts at passages 2 (lanes 1 and 2) and 4 (lanes 3 and 4) with indicated antibodies. Western blots of Rb phosphorylation sites (Ser780, Ser807/811, and Thr821) are shown in the bottom three panels.

(B) Expression analysis of indicated genes by RT-PCR from total MEF RNA at passages 2 (lanes 2 and 3) and 4 (lanes 4 and 5). Lane 1: 1 kb ladder II (Gene Choice, #62-6108-28). Lane 6: water control (ct-). All oligonucleotides used are listed in Table S1.

HPV-E7 in DKO MEFs would rescue the proliferation defect (Figure 7A, left panel). Expression of HPV-E7 not only rescued the proliferation defect, but it also restored the protein levels of Cdc2 and cyclin A2 in DKOs to levels comparable to those of wild-type MEFs (Figure 7A, right panel). Although *p27* RNA and Cdc2 protein expression is reduced in DKOs, we wanted to investigate if the loss of p27 would rescue proliferation since we have shown that Cdc2 activity is controlled by p27 and can regulate the G1/S transition in the absence of Cdk2 (Aleem et al., 2005). We generated TKOs, and, similar to what is seen with DKOs, $Cdk2^{-/-}Cdk4^{-/-}p27^{-/-}$ embryos were normal at E13.5 and died around E15.5 (data not shown). TKO $Cdk2^{-/-}Cdk4^{-/-}p27^{-/-}$ MEFs were analyzed, and we found that the loss of p27 did not rescue the proliferation defects of the DKO MEFs (Figure 7B). To verify that the proliferation defect in the DKOs is directly related to the loss of Cdk2, we expressed Cdk2-HA in DKO MEFs, thereby generating "$Cdk4^{-/-}$" MEFs. As expected, expression of Cdk2 in DKO MEFs restored proliferation in DKO MEFs to levels comparable to wild-type MEFs (Figure 7B). We also investigated if the premature senescence phenotype was correlated to Rb functions. Expression of HPV-E7 or Cdk2 restored the levels of senescence in DKO MEFs to wild-type levels (Figure 7C). In addition, spontaneous immortalization by passaging MEFs according to the 3T3 protocol (Todaro and Green, 1963) was analyzed. DKO and TKO MEFs were unable to become immortalized and stopped growing after ~10 passages (Figure 7D). Expression of HPV-E7 restored the immortalization of DKOs to wild-type levels.

These experiments are based on the fact that HPV-E7 inactivates Rb, but there have been indications that HPV-E7 might have also other functions that could influence the outcome of our experiments (for a review, see Münger and Howley, 2002). Therefore, we made use of a number of HPV-E7 mutants, some of which are unable to bind Rb (residues 22–26 of HPV-E7 include the core Rb binding site [LXCXE]). None of the HPV-E7 mutants defective in Rb binding (Δ21–24, C24G, E26G) rescued the proliferation (Figure 7E) or immortalization (data not shown) of DKO MEFs; however, other HPV-E7 mutants (Δ1–6 [amino-terminal CR1 homology domain necessary for cellular transformation], C91S [carboxyl-terminal zinc binding domain of E7 implicated in protein dimerization and stability]) partially rescued the proliferation of DKO MEFs (Figure 7E) but did not rescue immortalization (data not shown). These HPV-E7 mutants confirm that, most likely, the loss of Rb phosphorylation by Cdk2 and Cdk4 and the resulting repression of E2F transcription are the primary causes of the observed cell cycle defect in DKO MEFs. Nevertheless, we cannot exclude that other functions of HPV-E7 contribute to the rescue too.

Discussion

In this study, we have investigated the genetic interactions and functional overlap of Cdk2 and Cdk4 in vivo. We have generated $Cdk2^{-/-}Cdk4^{-/-}$ DKOs and observed that they die in utero around E15, most likely as a result of heart defects. The loss of Cdk2 and Cdk4 causes hypophosphorylation of Rb, which leads to repression of E2F-target gene expression. For example, Cdc2 and cyclin A2 cease to be expressed, resulting in a cell cycle defect. This most likely caused reduced proliferation, a premature senescent phenotype, and resistance to immortalization in $Cdk2^{-/-}Cdk4^{-/-}$ cells. To our knowledge, this is the first time that Cdk2 and Cdk4 are shown to be important for the regulation of Rb in vivo by using genetics, and that, indirectly, they are essential for Cdc2 expression.

Recently, using $Cdk2^{-/-}p27^{-/-}$ mice, we have shown that Cdc2 can compensate for the loss of Cdk2 (Aleem et al., 2005). Cdc2 interacts with cyclin E (Aleem et al., 2005; Koff et al., 1991) and is able to promote S phase entry. If Cdc2 is able to compensate for Cdk2, why is Cdc2 unable to rescue $Cdk2^{-/-}Cdk4^{-/-}$ mutants? Our results suggest that Cdc2 expression is turned off in DKOs because *Cdc2* transcription is regulated by E2Fs (Dalton, 1992). E2F regulation of Cdc2 was previously known, but given the fact that Cdc2 protein levels are constant and high, the importance of this kind of Cdc2 regulation was overlooked. Our results indicate that there is coupling of the G1 phase with mitosis through the transcriptional regulation of Cdc2: Cdk2 and Cdk4 control the expression of Cdc2 (through Rb/E2F). Our experiments with $Cdk2^{-/-}Cdk4^{-/-}$ DKOs suggest that Rb/E2F control of *Cdc2* expression is essential in vivo. Most likely, $Cdk2^{-/-}Cdk4^{-/-}$ mutants die because Cdc2 expression is lost at the same time. Therefore, the transcriptional

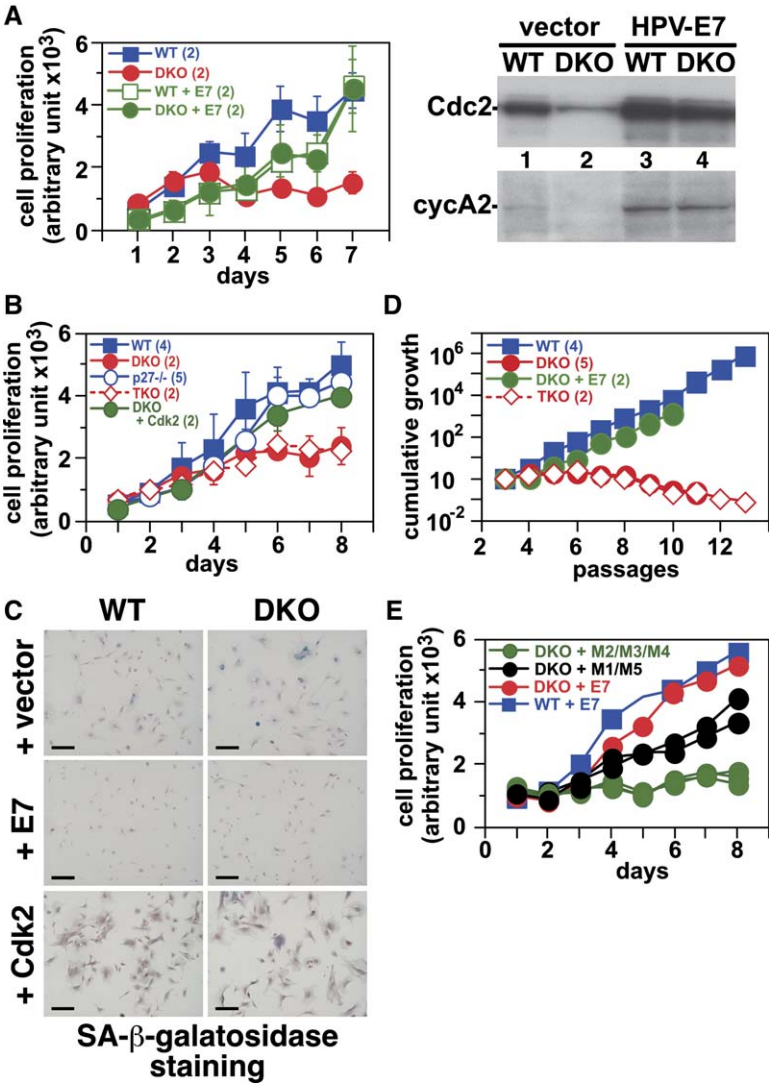

Figure 7. MEF Proliferation Defect Is Rescued by HPV16-E7

(A) Proliferation analysis of MEFs infected with HPV16-E7 at passage 4. Proliferation was analyzed for 7 days with AlamarBlue assays (left panel). Noninfected MEFs or MEFs infected with control vector (data not shown) behave similarly. Cells were harvested after selection, extracts were prepared, and Western blots were performed with indicated antibodies (right panel). Error bars represent the standard deviation of the data from the clone number indicated in the figure: WT, DKO, WT + E7, DKO + E7 (two clones each).

(B) Proliferation analysis at passage 2 of TKO *Cdk2*$^{-/-}$*Cdk4*$^{-/-}$*p27*$^{-/-}$ MEFs (TKO) and MEFs infected with *Cdk2-HA*. MEFs infected with control vector (data not shown) behave similarly to wild-type or *p27*$^{-/-}$ MEFs. Error bars represent the standard deviation of the data from the clone number indicated in the figure: WT (four clones), DKO (2 clones), p27$^{-/-}$ (five clones), TKO (two clones), DKO + Cdk2 (two clones).

(C) SA-β-galactosidase staining of wild-type MEFs (left column) and DKO MEFs (right column) infected with control vector, HPV16-E7, or *Cdk2-HA* at passage 4 as described in Figure 5 (the scale bar is 200 μm). Error bars represent the standard deviation of the data from the clone number indicated in the figure: WT (four clones), DKO (five clones), DKO + E7 (two clones), TKO (two clones).

(D) Immortalization of wild-type, DKO, TKO, and HPV16-E7-infected DKO MEFs by using the 3T3 protocol. Cumulative cell numbers over 10–13 passages were plotted; therefore, crisis, which occurred around passages 6–10 is not easily apparent. DKOs infected with control vector behave similarly to DKO MEFs, and wild-type MEFs infected with HPV16-E7 behave similarly to wild-type MEFs (data not shown).

(E) Proliferation analysis of wild-type and DKO MEFs infected with HPV16-E7 or HPV16-E7 mutants (M1, Δ1–4; M2, Δ21–24; M3, C24G; M4, E26G; M5, C91S) at passage 4. Mutants M2–M4 affect HPV16-E7 Rb binding. Wild-type MEFs infected with HPV16-E7 mutants (data not shown) behave similarly to wild-type MEFs.

control of *Cdc2* is important for its protein expression levels in vivo. It remains to be seen whether expression of Cdc2 from a heterologous promoter would rescue some of the *Cdk2*$^{-/-}$*Cdk4*$^{-/-}$ phenotypes.

Cdk2$^{-/-}$*Cdk4*$^{-/-}$ cells display proliferation defects, but why can they proliferate at all? In early embryogenesis, proliferation seems close to normal, and Rb is phosphorylated on serine 780 (see Figure 4, lane 2) in *Cdk2*$^{-/-}$ *Cdk4*$^{-/-}$ mutants. We can envision two possibilities for the phosphorylation of Rb in the absence of Cdk2 and Cdk4, which would involve Cdk6 and/or Cdc2. In the absence of Cdk4, we have detected more cyclin D1/Cdk6 complexes in comparison to wild-type (see Figure 4, bottom panel). These cyclin D1/Cdk6 complexes most likely contribute to the phosphorylation of Rb. Nevertheless, in E16.5 embryos, we did not detect cyclin D1 complexes anymore because cyclin D1 protein expression is decreased (Figure 4, lane 6). Similarly, it is possible that Cdc2 complexes contribute to the phosphorylation of Rb since Cdc2 displays a substrate specificity comparable to that of Cdk2. Cdc2 protein (see Figure 4, lane 2), complexes, and activity were detectable in early DKO and wild-type embryos. At a time when phosphorylation of Rb starts to decline, the E2F-target gene transcription decreases, and, as a consequence, Cdc2 might not be able to phosphorylate Rb as efficiently, enhancing the negative feedback loop to arrest the cell cycle. We cannot exclude that another (unknown) kinase contributes to Rb phosphorylation in early embryogenesis, but we believe that Cdk6 and/or Cdc2 are the most likely candidates.

Cdk2$^{-/-}$*Cdk6*$^{-/-}$ DKO mice are viable (Malumbres et al., 2004), and, in contrast, we have shown here that *Cdk2*$^{-/-}$*Cdk4*$^{-/-}$ mutants are embryonic lethal. This indicates intrinsic differences between Cdk4 (in the case of *Cdk2*$^{-/-}$*Cdk6*$^{-/-}$) and Cdk6 (in the case of *Cdk2*$^{-/-}$ *Cdk4*$^{-/-}$). Cdk4 or Cdk6 are required for viability since *Cdk4*$^{-/-}$*Cdk6*$^{-/-}$ mutants are lethal (Malumbres et al., 2004). One could envision that this is because the expression of Cdk6 is much more restricted compared to Cdk4, giving a potential explanation for the heart

defect; however, in MEFs, that is actually not the case. Therefore, it is likely that Cdk4 can phosphorylate Rb more efficiently than Cdk6, or that Cdk4 has other substrates compared to Cdk6. It will be interesting to identify these molecular differences between Cdk4 and Cdk6 in the future.

Our results indicate the importance of an in vivo functional overlap between Cdk2 and Cdk4 in the regulation of the Rb/E2F pathway during normal development. It will be interesting to investigate whether the Cdk2/Cdk4 redundancy is also essential during tumorigenesis since silencing of Cdk2 in certain tumor cell lines had no effect on the proliferation of these cells (Tetsu and McCormick, 2003).

Experimental Procedures

Generation of *Cdk2*$^{-/-}$*Cdk4*$^{-/-}$ Mice

Cdk2$^{+/-}$ mice were crossed with *Cdk4*$^{+/-}$ mice (Berthet et al., 2003; Tsutsui et al., 1999). Heterozygous offspring *Cdk2*$^{+/-}$*Cdk4*$^{+/-trans}$ mice were backcrossed with C57BL/6 mice to produce *Cdk2*$^{+/-}$*Cdk4*$^{+/-cis}$ mice, which were, in turn, intercrossed to generate homozygous mutant *Cdk2*$^{-/-}$*Cdk4*$^{-/-}$ animals. The mice used in this study were of mixed C57BL/6 × 129S1/SvImJ background. Mice were routinely genotyped by isolating tail DNA with HOTshot lysis (Truett et al., 2000) and PCR with *Cdk2* oligonucleotides (F: 5′-GTGA CCCTGTGGTACCGAGCACCTG-3′ [PKO0292]; R: 5′-GGTTTTGCTC TTGGATGTGGGCATGG-3′ [PKO0344]; Neo: 5′-CCCGTGATATTGC TGAAGAGCTTGGCGG-3′ [PKO0294]) and *Cdk4* oligonucleotides (F: 5′-CGGAAGGCAGAGATTCGCTTAT-3′ [PKO0104]; R: 5′-CCAGC CTGAAGCTAAGAGTAGCTGT-3′ [PKO0105]; Neo [PKO0294]) for 30 cycles at 94°C for 30 s and 62°C for 60 s. Southern blots were performed occasionally to confirm genotyping, by using *Cdk2* 5′ or 3′ probes and the *Cdk4* 5′ probe previously described (Berthet et al., 2003; Tsutsui et al., 1999). *Cdk2*$^{+/-}$*Cdk4*$^{+/-cis}$ mice were crossed to *p27*$^{+/-}$ (Kiyokawa et al., 1996) to generate TKOs. Genotyping of p27 was performed as described (Aleem et al., 2005). Mice were group-housed under standard conditions with food and water available ad libitum and were maintained on a 12 hr light/dark cycle. Mice were fed a standard chow diet containing 6% crude fat and were treated in compliance with the National Institutes of Health guidelines for animal care and use.

Histopathology and Immunohistochemistry

Organs were dissected, fixed in 10% neutral buffered formalin (Accustain from Sigma-Aldrich, USA), and embedded in paraffin. Sections were stained with hematoxylin and eosin (H&E). For analysis of proliferation, mice were injected intraperitoneally with BrdU (100 mg bromodeoxyuridine per kilogram body weight), and tissues were collected after 1 hr, fixed in 70% ethanol, and embedded in paraffin. Paraffin sections were stained with antibodies against BrdU (DAKO, Cat# M0744) at a concentration of 27 μg/ml, followed by detection with the Vectastain ABC kit (Vector Laboratories, CA, USA). For flow cytometry analysis, BrdU-injected embryos were harvested as described above, and liver and brain were isolated. Cell suspensions were prepared as described below. Cells were counted and fixed in 70% ethanol. BrdU and propidium iodide staining were performed as described (Berthet et al., 2003).

Analysis of Hematopoietic Progenitors in Fetal Liver

Fetal livers were dissected from E14.5 embryos, dissociated, and passed through fine mesh (BD Falcon, #352340) to generate a single cell suspension. The cells were resuspended at a density of 1×10^6 cells/100 μl in PBS with 0.1% BSA (Sigma-Aldrich, St. Louis, MO), and they were stained with fluorescein isothiocyanate-conjugated CD34 (RAM34), phycoerythrin-conjugated anti-c-Kit (2B8), phycoerythrin-Cy5-conjugated FcγRII/III (2.4G2; Pharmingen, San Diego, CA), and allophycocyanin-conjugated anti-Sca-1 (Ly-6A/E) monoclonal antibodies (eBioscience, San Diego, CA) to distinguish HSC, CMP, GMP, and MEP populations, respectively. To exclude terminally differentiated hematopoietic cells, cells were stained with biotinylated antibodies specific for the following lineage markers: CD3ε, CD4, CD8, B220, and TER119 (Pharmingen, San Diego, CA). Biotinylated IL-7Rα (A7R34) antibody was added to this cocktail to exclude fetal liver common lymphoid progenitors (CLP), and the cells were then stained with avidin-PerCP-Cy5.5. Throughout staining, the cells were kept at 4°C, and the antibodies were used at a concentration of 0.5 μg/1×10^6 cells. All cell populations were analyzed by using a FACS LSRII (Becton Dickinson Immunocytometry, Mountain View, CA).

The proliferative response of fetal liver cells to hematopoietic growth factors was measured with a ^{3}H-thymidine proliferation assay. Cells were washed three times in complete medium and plated at 5×10^3 cells per well per 100 μl in triplicate in either complete medium with no growth factors or complete medium with 100 ng/ml mSCF, 30 ng/ml mIL-3, 100 ng/ml hFlt-3 ligand, and 50 ng/ml mIL-6 (all growth factors from Peprotech, Rocky Hill, NJ, USA). After 2 and 5 days in culture, cells were pulsed with 1 μCi ^{3}H-thymidine per well (6.7 Ci/mmol, Perkin Elmer Life Sciences, Inc., Boston, MA) and incubated for an additional 16 hr. To measure ^{3}H-thymidine incorporation, the cells were harvested onto glass-fiber filtermats (Filtermat A; Wallac Oy, Turku, Finland) by using a Tomtech Harvester 96 (Tomtech, Inc., Orange, CT), and the filters were allowed to dry overnight. Radioactivity was counted by using BetaPlate Scint liquid scintillation fluid (Perkin Elmer) and a 1205 Betaplate liquid scintillation counter (LKB Wallac, Perkin Elmer).

Isolation and Culture of Embryonic Fibroblasts

Fibroblasts were prepared from embryos at 13.5 days postcoitum as described previously (Berthet et al., 2003). The cell suspension from each individual embryo was seeded in 100 mm culture dishes (passage 0). MEFs were routinely cultured in a humidified 5% CO_2 atmosphere at 37°C in Dulbecco's modified minimum essential medium (DMEM, Invitrogen, #10569-010) supplemented with 10% (w/v) fetal calf serum (FBS; Gemini Bio-Products, #100-106) and 1% penicillin/streptomycin (Invitrogen, #15140-122). Proliferation of MEFs was analyzed in 96-well plates with 1500 cells/well (triplicate for each clone/day) and scored by using the AlamarBlue assay (Biosource, DAL1100) (Ahmed et al., 1994). Complete medium with 10% AlamarBlue was added to each well, and a fluorescent reading was carried out 4 hr later. Cell cycle synchronization by serum starvation and BrdU incorporation were performed as described (Berthet et al., 2003). Cells were harvested at the indicated time points after serum addition, washed with cold PBS and frozen in nitrogen for protein or RNA analysis, or fixed in 70% ethanol for flow cytometry analysis. Cell cycle analysis after propidium iodide and BrdU staining was performed as described (Berthet et al., 2003). Senescence analysis has been performed according to the original protocol (Dimri et al., 1995). A total of 10^4 cells were plated in a Lab-Tek II chamber slide (Nalgen Nunc International, #154461) and 24 hr later were washed with PBS, fixed in 2% formaldeyde/0.2% glutaraldehyde for 5 min at room temperature, washed with PBS, and incubated overnight at 37°C with 0.2 μm filtered SA-β-galactosidase solution (PBS/citric acid [pH 6], 5 mM potassium ferrocyanide, 5 mM potassium ferricyanide, 150 mM NaCl, 2 mM $MgCl_2$, 1 mg/ml X-Gal [Promega, #V3941]). Slides were counterstained with 0.1% Neutral Red (83% Neutral Red dye; Matheson, Coleman and Bell, #B36-NX260) in dH_2O for 1 min, rinsed, and dehydrated in 100% ethanol (three changes). Then slides were placed in Xylene (four changes), and coverslips were mounted with Permount (Fisher).

Retroviral Infection of MEFs

The human *Cdk2-HA* ORF and viral HPV16-E7 were cloned into the BamHI site of the retroviral vector pBabe (PKB722 and PKB841, respectively). HPV16-E7 mutants (Δ1–4, Δ21–24, C24G, E26G, C91S) are cloned into retroviral pBabe vector and were a kind gift of Karl Münger. Plasmids were transfected into the packaging cell line Eco Phoenix by using Lipofectamine 2000 (Invitrogen, #11668-019). After 48 and 72 hr, MEFs were infected with 3 ml of the supernatant of Eco Phoenix cells containing viral particles in the presence of 8 μg/ml polybrene (Sigma, # H-9268) and were allowed to grow for 2 more days. The infected MEFs were selected for 4 days with 2.5 μg/ml puromycin (Sigma, # 82595) and were plated for the experiments.

Protein Analysis

Proteins from embryos or MEFs were isolated at 4°C by using a Teflon potter homogenizer and the following lysis buffer: 50 mM HEPES

(pH 7), 150 mM NaCl, 2.5 mM EGTA, 1 mM EDTA, 10 mM β-glycerol phosphate, 0.1% Tween 20, 10% glycerol, 1 mM DTT, 2 mM NaF, 1× protease inhibitors (10 μg/ml each of leupeptin, chymostatin, and pepstatin [Chemicon, Temecula, CA]). Lysates were centrifuged for 45 min at 18,000 × g at 4ºC, and supernatants were frozen in liquid nitrogen. Protein concentrations were determined by using the Bradford protein assay (Biorad, #500-0006). Lysates were analyzed by immunoblotting, immunoprecipitation, and kinase assays by using the substrate histone H1 as previously described (Berthet et al., 2003). Affinity-purified antibodies against Cdk2, Cdc2, Cdk4, Cdk6, and cyclin B1 have been described (Berthet et al., 2003). Other antibodies are commercially available: rabbit anti-cyclin A (0.2 μg/ml, Santa Cruz, H-432, #Sc-751), rabbit anti-cyclin D1 (2 μg/ml, NeoMarkers, #RB-010-P), rabbit anti-Cdk4 (0.1 μg/ml, Clontech, #3517-1), rabbit anti-E2F1 (0.4 μg/ml, Santa Cruz, C-20, #Sc-193), rabbit anti-p27 (0.5 μg/ml, Zymed, #71-9600), mouse anti-Rb (0.2 μg/ml, BD PharMingen, G3-245, #554136), rabbit anti-phospho-Rb^{Ser780}, $Rb^{S807/811}$ (1:1000, Cell Signaling, #9307/8), rabbit anti-phospho-Rb^{Thr821} (1:1000, Biosource, #44-582G), goat anti-β-actin (0.4 μg/ml, Santa Cruz, I-19, #Sc-1616). For immunoprecipitation, 10 μl antibodies conjugated to agarose beads were used (available at Santa Cruz, #Sc-xxx-AC) as well as anti-Rb-agarose beads (Santa Cruz, IF8, #Sc-102) or $p13^{Suc1}$-agarose beads (Upstate Biotechnology, #14-132).

RNA Analysis

Total RNA was isolated from primary MEFs by using the Trizol reagent (Life Technologies, #15596) according to the manufacturer's instructions. cDNAs were generated with reverse transcriptase (SuperScript II, Invitrogen, #18064014) by using 1 μg total RNA at 42ºC for 1 hr and 1.25 μM oligo-dT_{16} primers according to the manufacturer's instructions. cDNAs were amplified by using specific primers (Table S1) for 25 cycles at 94ºC for 30 s, 55ºC for 30 s, and 72ºC for 60 s. PCR products were analyzed by electrophoresis on 3% agarose gels.

Supplemental Data

Supplemental Data including descriptions of ocular lesions, apoptosis, the activity of Cdk/cyclin complexes, and FACS analysis of MEFs are available at http://www.developmentalcell.com/cgi/content/full/10/5/563/DC1/.

Acknowledgments

The authors thank Nancy Jenkins and Neal Copeland for advice, discussion, reagents, and support. We also thank Barbara Shankle and Carlton Briggs for technical help; Karen Stull, Matt McCollum, and Angie Smith for animal care; Kathleen Noer and Roberta Matthai for FACS analysis; and Keith Rogers, Roberta Smith, Jen Matta, and Miriam Anver (http://web/rtp/lasp/phl/) for the analysis of mouse pathology. We are grateful to Brad St. Croix and Ira Daar for providing equipment and reagents, and to Karl Münger for HPV-E7 mutants. We really appreciated the help of Debbie Hodge, Shyam Sharan, Eiman Aleem, Karlyne Reilly, Esta Sterneck, Lino Tessarollo, Enzo Coppola, Terry Yamaguchi, and the Kaldis lab for discussions and collaboration. We are thankful to Deborah Morrison, Shyam Sharan, V.C. Padmakumar, Weimin Li, Jean-Pierre Magaud, Jacques Samarut, Neil Segil, and Neal Copeland for comments on the manuscript. C.B. dedicates this paper to Sophie for her support and to Manon, Agathe, and Emeric. This research was supported by the Intramural Research Program of the National Institutes of Health, National Cancer Institute, Center for Cancer Research.

Received: November 17, 2005
Revised: March 6, 2006
Accepted: March 14, 2006
Published: May 8, 2006

References

Ahmed, S.A., Gogal, R.M., Jr., and Walsh, J.E. (1994). A new rapid and simple non-radioactive assay to monitor and determine the proliferation of lymphocytes: an alternative to ^3H thymidine incorporation assay. J. Immunol. Methods *170*, 211–224.

Akashi, K., Traver, D., Miyamoto, T., and Weissman, I.L. (2000). A clonogenic common myeloid progenitor that gives rise to all myeloid lineages. Nature *404*, 193–197.

Aleem, E., Kiyokawa, H., and Kaldis, P. (2005). Cdc2-cyclin E complexes regulate the G1/S phase transition. Nat. Cell Biol. *7*, 831–836.

Bartek, J., Bartkova, J., and Lukas, J. (1996). The retinoblastoma protein pathway and the restriction point. Curr. Opin. Cell Biol. *8*, 805–814.

Berthet, C., Aleem, E., Coppola, V., Tessarollo, L., and Kaldis, P. (2003). Cdk2 knockout mice are viable. Curr. Biol. *13*, 1775–1785.

Dalton, S. (1992). Cell cycle regulation of the human *cdc2* gene. EMBO J. *11*, 1797–1804.

Dimri, G.P., Lee, X., Basile, G., Acosta, M., Scott, G., Roskelley, C., Medrano, E.E., Linskens, M., Rubelj, I., Pereira-Smith, O., et al. (1995). A biomarker that identifies senescent human cells in culture and in aging skin in vivo. Proc. Natl. Acad. Sci. USA *92*, 9363–9367.

Ezhevsky, S.A., Ho, A., Becker-Hapak, M., Davis, P.K., and Dowdy, S.F. (2001). Differential regulation of retinoblastoma tumor suppressor protein by G1 cyclin-dependent kinase complexes in vivo. Mol. Cell. Biol. *21*, 4773–4784.

Fantl, V., Stamp, G., Andrews, A., Rosewell, I., and Dickson, C. (1995). Mice lacking cyclin D1 are small and show defects in eye and mammary gland development. Genes Dev. *9*, 2364–2372.

Geng, Y., Yu, Q., Sicinska, E., Das, M., Schneider, J.E., Bhattacharya, S., Rideout, W.M., Bronson, R.T., Gardner, H., and Sicinski, P. (2003). Cyclin E ablation in the mouse. Cell *114*, 431–443.

Harbour, J.W., and Dean, D.C. (2000). The Rb/E2F pathway: expanding roles and emerging paradigms. Genes Dev. *14*, 2393–2409.

Harbour, J.W., Luo, R.X., Dei Santi, A., Postigo, A.A., and Dean, D.C. (1999). Cdk phosphorylation triggers sequential intramolecular interactions that progressively block Rb functions as cells move through G1. Cell *98*, 859–869.

Kingsley, P.D., Malik, J., Fantauzzo, K.A., and Palis, J. (2004). Yolk sac-derived primitive erythroblasts enucleate during mammalian embryogenesis. Blood *104*, 19–25.

Kiyokawa, H., Kineman, R.D., Manova-Todorova, K.O., Soares, V.C., Hoffman, E.S., Ono, M., Khanam, D., Hayday, A.C., Frohman, L.A., and Koff, A. (1996). Enhanced growth of mice lacking the cyclin-dependent kinase inhibitor function of $p27^{Kip1}$. Cell *85*, 721–732.

Koff, A., Cross, F., Fisher, A., Schumacher, J., Leguellec, K., Philippe, M., and Roberts, J.M. (1991). Human cyclin E, a new cyclin that interacts with two members of the CDC2 gene family. Cell *66*, 1217–1228.

Kozar, K., Ciemerych, M.A., Rebel, V.I., Shigematsu, H., Zagozdzon, A., Sicinska, E., Geng, Y., Yu, Q., Bhattacharya, S., Bronson, R.T., et al. (2004). Mouse development and cell proliferation in the absence of D-cyclins. Cell *118*, 477–491.

Lundberg, A.S., and Weinberg, R.A. (1998). Functional inactivation of the retinoblastoma protein requires sequential modification by at least two distinct cyclin-cdk complexes. Mol. Cell. Biol. *18*, 753–761.

Malumbres, M., and Barbacid, M. (2005). Mammalian cyclin-dependent kinases. Trends Biochem. Sci. *30*, 630–641.

Malumbres, M., Sotillo, R., Santamaria, D., Galan, J., Cerezo, A., Ortega, S., Dubus, P., and Barbacid, M. (2004). Mammalian cells cycle without the D-type cyclin-dependent kinases Cdk4 and Cdk6. Cell *118*, 493–504.

Mittnacht, S. (1998). Control of pRB phosphorylation. Curr. Opin. Genet. Dev. *8*, 21–27.

Morgan, D.O. (1997). Cyclin-dependent kinases: engines, clocks, and microprocessors. Annu. Rev. Cell Dev. Biol. *13*, 261–291.

Münger, K., and Howley, P.M. (2002). Human papillomavirus immortalization and transformation functions. Virus Res. *89*, 213–228.

Ortega, S., Prieto, I., Odajima, J., Martin, A., Dubus, P., Sotillo, R., Barbero, J.L., Malumbres, M., and Barbacid, M. (2003). Cyclin-dependent kinase 2 is essential for meiosis but not for mitotic cell division in mice. Nat. Genet. *35*, 25–31.

Parisi, T., Beck, A.R., Rougier, N., McNeil, T., Lucian, L., Werb, Z., and Amati, B. (2003). Cyclins E1 and E2 are required for endoreplication in placental trophoblast giant cells. EMBO J. *22*, 4794–4803.

Rane, S.G., Dubus, P., Mettus, R.V., Galbreath, E.J., Boden, G., Reddy, E.P., and Barbacid, M. (1999). Loss of Cdk4 expression causes insulin-deficient diabetes and Cdk4 activation results in β-islet cell hyperplasia. Nat. Genet. *22*, 44–52.

Ruas, M., and Peters, G. (1998). The $p16^{INK4a/CDKN2A}$ tumor suppressor and its relatives. Biochim. Biophys. Acta *1378*, F115–F177.

Sherr, C.J. (2001). The INK4a/ARF network in tumour suppression. Nat. Rev. Mol. Cell Biol. *2*, 731–737.

Sherr, C.J., and Roberts, J.M. (1999). CDK inhibitors: positive and negative regulators of G_1-phase progression. Genes Dev. *13*, 1501–1512.

Sicinski, P., Donaher, J.L., Parker, S.B., Li, T., Fazeli, A., Gardner, H., Haslam, S.Z., Bronson, R.T., Elledge, S.J., and Weinberg, R.A. (1995). Cyclin D1 provides a link between development and oncogenesis in the retina and breast. Cell *82*, 621–630.

Sicinski, P., Donaher, J.L., Geng, Y., Parker, S.B., Gardner, H., Park, M.Y., Robker, R.L., Richards, J.S., McGinnis, L.K., Biggers, J.D., et al. (1996). Cyclin D2 is an FSH-responsive gene involved in gonadal cell proliferation and oncogenesis. Nature *384*, 470–474.

Silver, L. (1995). Mouse Genetics (Oxford, UK: Oxford University Press).

Tetsu, O., and McCormick, F. (2003). Proliferation of cancer cells despite CDK2 inhibition. Cancer Cell *3*, 233–245.

Todaro, G.J., and Green, H. (1963). Quantitative studies of the growth of mouse embryo cells in culture and their development into established lines. J. Cell Biol. *17*, 299–313.

Trimarchi, J.M., and Lees, J.A. (2002). Sibling rivalry in the E2F family. Nat. Rev. Mol. Cell Biol. *3*, 11–20.

Truett, G.E., Heeger, P., Mynatt, R.L., Truett, A.A., Walker, J.A., and Warman, M.L. (2000). Preparation of PCR-quality mouse genomic DNA with hot sodium hydroxide and tris (HotSHOT). Biotechniques *29*, 52, 54.

Tsutsui, T., Hesabi, B., Moons, D.S., Pandolfi, P.P., Hansel, K.S., Koff, A., and Kiyokawa, H. (1999). Targeted disruption of CDK4 delays cell cycle entry with enhanced $p27^{Kip1}$ activity. Mol. Cell. Biol. *19*, 7011–7019.

Weinberg, R.A. (1995). The Retinoblastoma protein and cell cycle control. Cell *81*, 323–330.

Zarkowska, T.U.S., Harlow, E., and Mittnacht, S. (1997). Monoclonal antibodies specific for underphosphorylated retinoblastoma protein identify a cell cycle regulated phosphorylation site targeted by cdks. Oncogene *14*, 249–254.